Landes Bioscience www.landesbioscience.com

Supplemental Material to:

Keisuke Ikawa, Ayaka Satou, Mitsuko Fukuhara, Shigeru Matsumura, Naoyuki Sugiyama, Hidemasa Goto, Mitsunori Fukuda, Masaki Inagaki, Yasushi Ishihama, and Fumiko Toyoshima

Inhibition of endocytic vesicle fusion by Plk1-mediated phosphorylation of vimentin during mitosis

Cell Cycle 2014; 13(1)
http://dx.doi.org/10.4161/cc.26866

http://www.landesbioscience.com/journals/cc/article/26866

Supplementary Information

Inhibition of endocytic vesicle fusion by Plk1-mediated phosphorylation of vimentin during mitosis

Keisuke Ikawa, Ayaka Satou, Mitsuko Fukuhara, Shigeru Matsumura, Naoyuki Sugiyama, Hidemasa Goto, Mitsunori Fukuda, Masaki Inagaki, Yasushi Ishihama, Fumiko Toyoshima

Supplementary Methods

GST-pull down assay for Rab5

M phase synchronized HeLa cells stably expressing GFP-Rab5A were lysed in lysis buffer (50mM Tris (pH 7.5), 10mM $MgCl_2$, 300mM NaCl, 1mM dithiothreitol, 0.5μg/ml leupeptin, 2μg/ml aprotinin, 10μg/ml phenylmethylsulfonyl fluoride, 2% IGEPAL). The cell lysates were centrifuged at 20,000g for 5 min, and the supernatants were incubated with recombinant GST (20μg) or recombinant GST-Rab5 binding domain (R5BD) of Rabaptin5 (20μg) for 30 min, and then incubated with glutathione sepharose beads (GE healthcare) for 30 minutes. The beads were washed three times with wash buffer (25mM Tris (pH 7.5), 30mM $MgCl_2$, 40mM NaCl, 1mM dithiothreitol, 0.5μg/ml leupeptin, 2μg/ml aprotinin, 10μg/ml phenylmethylsulfonyl fluoride) and subjected to immunoblotting with anti-GFP antibodies.

Table S1. Phosphopeptides in the early endosome fractions incubated with His-Plk1-WT

AccNum	Protein name	phospho-site	sequence
1433E_HUMAN	14-3-3 protein epsilon	S148	EAAENSLVAYK
A1AT_HUMAN	Alpha-1-antitrypsin	S325	LSITGTYDLKSVLGQLGITKVFSNGADLSGVTEEAPLKLSKAVHK
A1AT_HUMAN	Alpha-1-antitrypsin	S405	SPLFMGKVVNPTQK
ACTB_HUMAN	Actin, cytoplasmic 1	S239	SYELPDGQVITIGNER
ALDOA_HUMAN	Fructose-bisphosphate aldolase A	S36	GILAADESTGSIAK
ANXA1_HUMAN	Annexin A1	S189	GDRSEDFGVNEDLADSDAR
ANXA1_HUMAN	Annexin A1	T169	DITSDTSGDFRNALLSLAK
ANXA1_HUMAN	Annexin A1	S182	DITSDTSGDFRNALLSLAK
ANXA1_HUMAN	Annexin A1	T141	RVFQKYTK
DCD_HUMAN	Dermcidin	S93	AVGGLGKLGKDAVEDLESVGKGAVHDVKDVLDS
DCD_HUMAN	Dermcidin	S108	AVGGLGKLGKDAVEDLESVGKGAVHDVKDVLDS
EF1A2_HUMAN	Elongation factor 1-alpha 2	S445	KSGGAGKVTK
EF1A2_HUMAN	Elongation factor 1-alpha 2	T452	KSGGAGKVTK
ENPL_HUMAN	Endoplasmin	S64	EEEAIQLDGLNASQIR
ERO1A_HUMAN	ERO1-like protein alpha	S143	LGAVDESLSEETQK
ERO1A_HUMAN	ERO1-like protein alpha	S145	LGAVDESLSEETQK
G3P_HUMAN	Glyceraldehyde-3-phosphate dehydrogenase	S241	VPTANVSVVDLTCR
G3P_HUMAN	Glyceraldehyde-3-phosphate dehydrogenase	T246	VPTANVSVVDLTCR
GRP78_HUMAN	78 kDa glucose-regulated protein	T85	NQLTSNPENTVFDAKR
GRP78_HUMAN	78 kDa glucose-regulated protein	T91	NQLTSNPENTVFDAKR
HS90B_HUMAN	Heat shock protein HSP 90-beta	S391	GVVDSEDLPLNISR
HSPB1_HUMAN	Heat shock protein beta-1	S82	QLSSGVSEIR
IMA2_HUMAN	Importin subunit alpha-2	S88	GINSSNVENQLQATQAAR
K1C13_HUMAN	Keratin, type I cytoskeletal 13	S427	MIGFPSSAGSVSPR
K1C13_HUMAN	Keratin, type I cytoskeletal 13	S7	LQSSSASYGGGFGGGSCQLGGGR
K1C13_HUMAN	Keratin, type I cytoskeletal 13	S453	TSDVRRP
NUCL_HUMAN	Nucleolin	T76	VAVATPAK
PDIA3_HUMAN	Protein disulfide-isomerase A3	T437	MDATANDVPSPYEVR
PDIA3_HUMAN	Protein disulfide-isomerase A3	T31	SDVLELTDDNFESR
PDIA3_HUMAN	Protein disulfide-isomerase A3	S209	PSHLTNKFEDK
PEX19_HUMAN	Peroxisomal biogenesis factor 19	S147	NATDLQNSSMSEEELTK
PEX19_HUMAN	Peroxisomal biogenesis factor 19	S149	NATDLQNSSMSEEELTK
POTEE_HUMAN	POTE ankyrin domain family member E	S89	SNVGASGDHDDSAMKTLR
POTEE_HUMAN	POTE ankyrin domain family member E	Y940	SYELPDGQVITIGNER
POTEE_HUMAN	POTE ankyrin domain family member E	T93	TLRNKMGK
RIC1_HUMAN	Protein RIC1 homolog	T960	QHATLLFNTALEQGK
RIC1_HUMAN	Protein RIC1 homolog	T965	QHATLLFNTALEQGK
RIC1_HUMAN	Protein RIC1 homolog	T64	SSTQFGSYK
SRPR_HUMAN	Signal recognition particle receptor subunit alpha	S297	GTGSGGQLQDLDCSSSDDEGAAQNSTKPSATK
VIME_HUMAN	Vimentin	S459	DGQVINETSQHHDDLE

The red characters represent phosphosites

Supplementary Figure 1

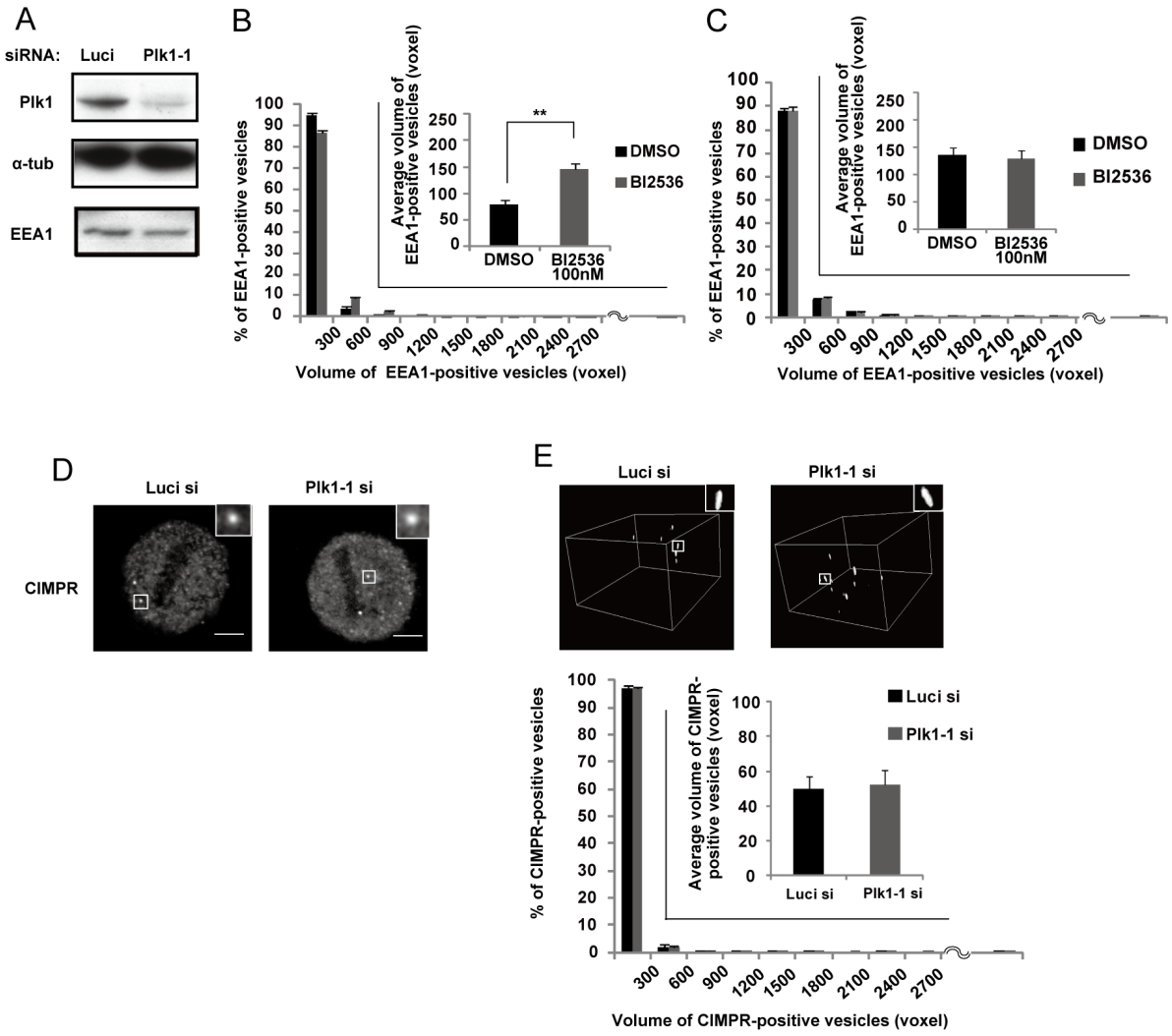

Supplementary Figure 2

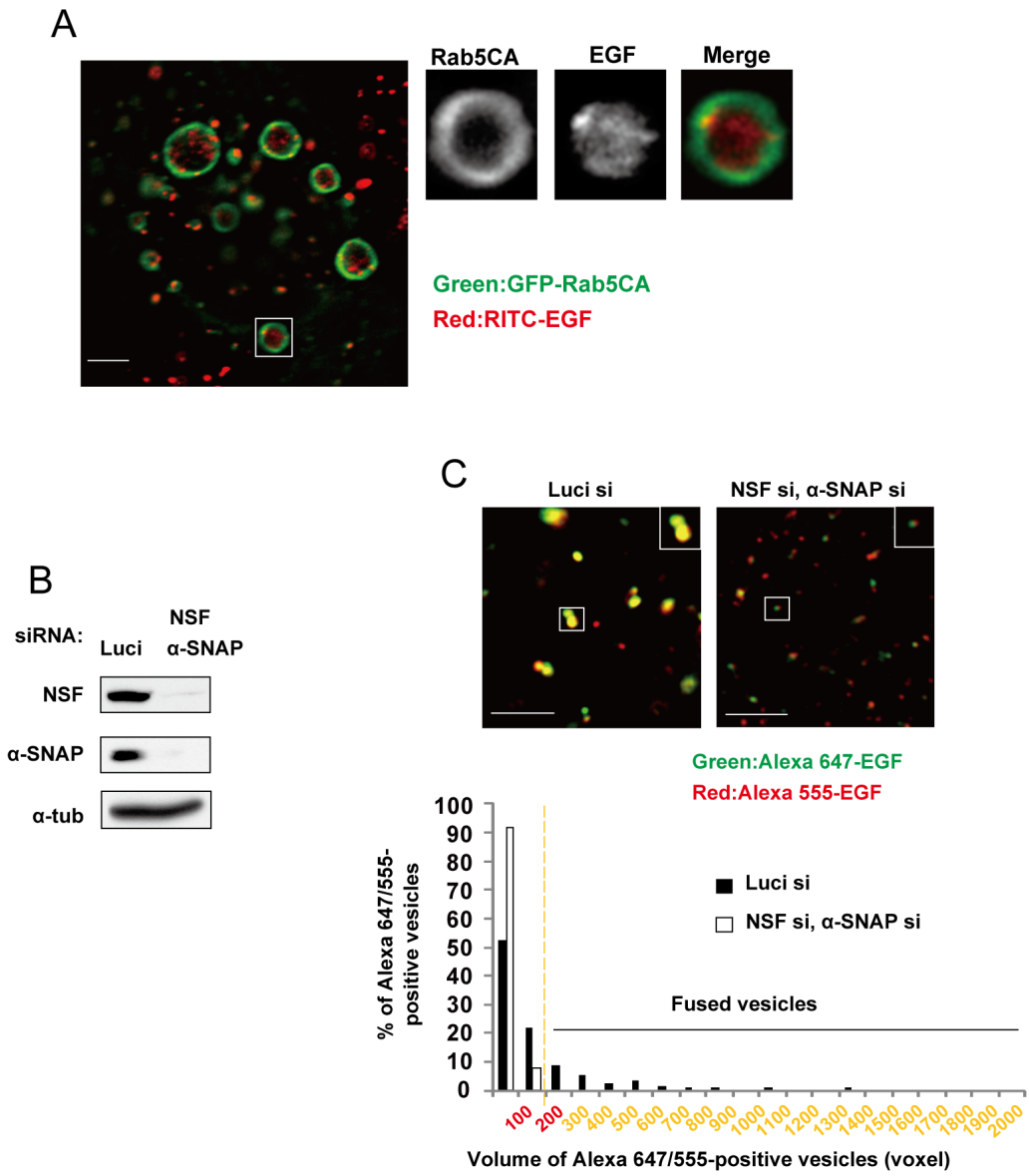

Supplementary Figure 3

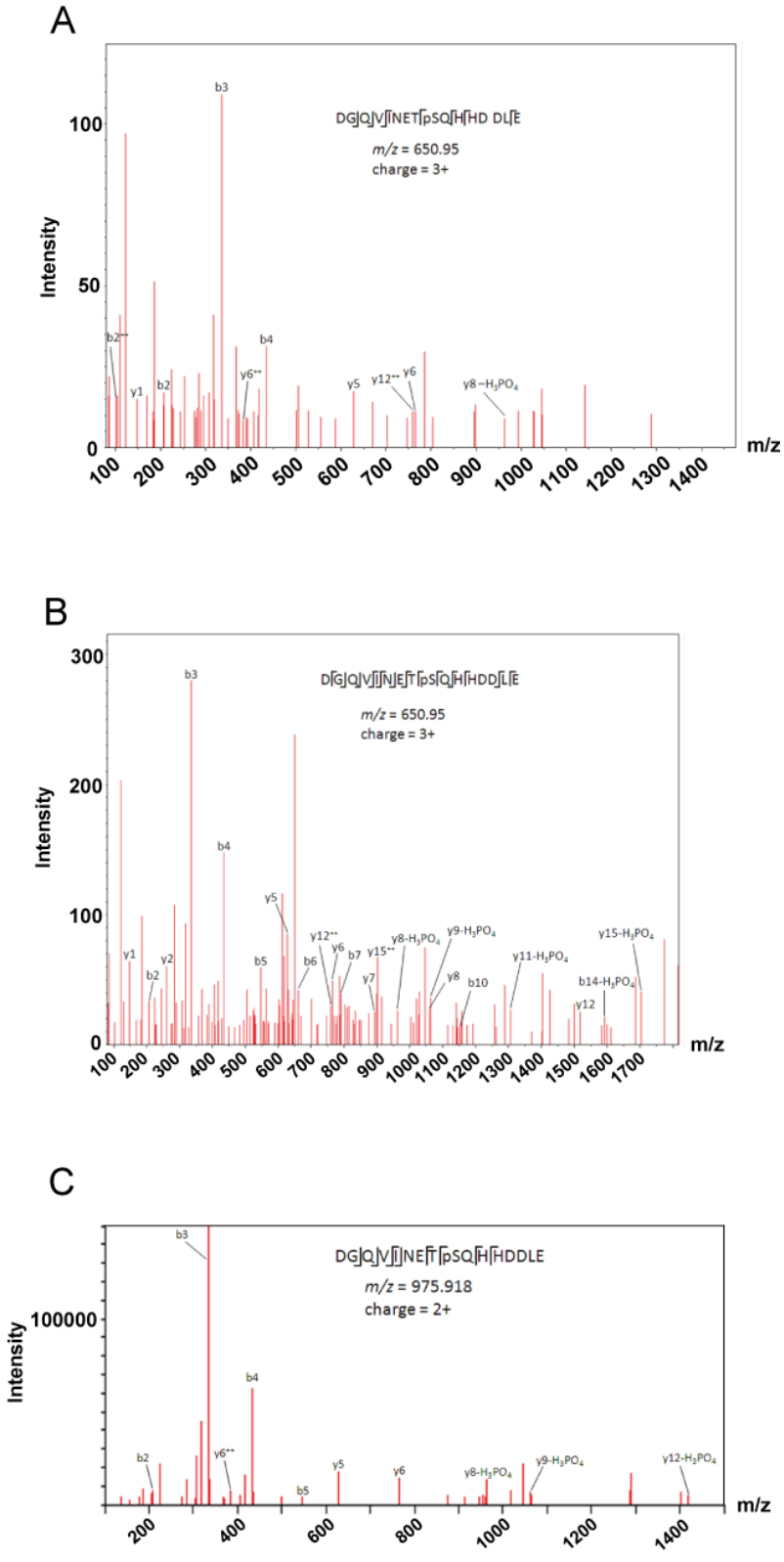

Supplementary Figure 4

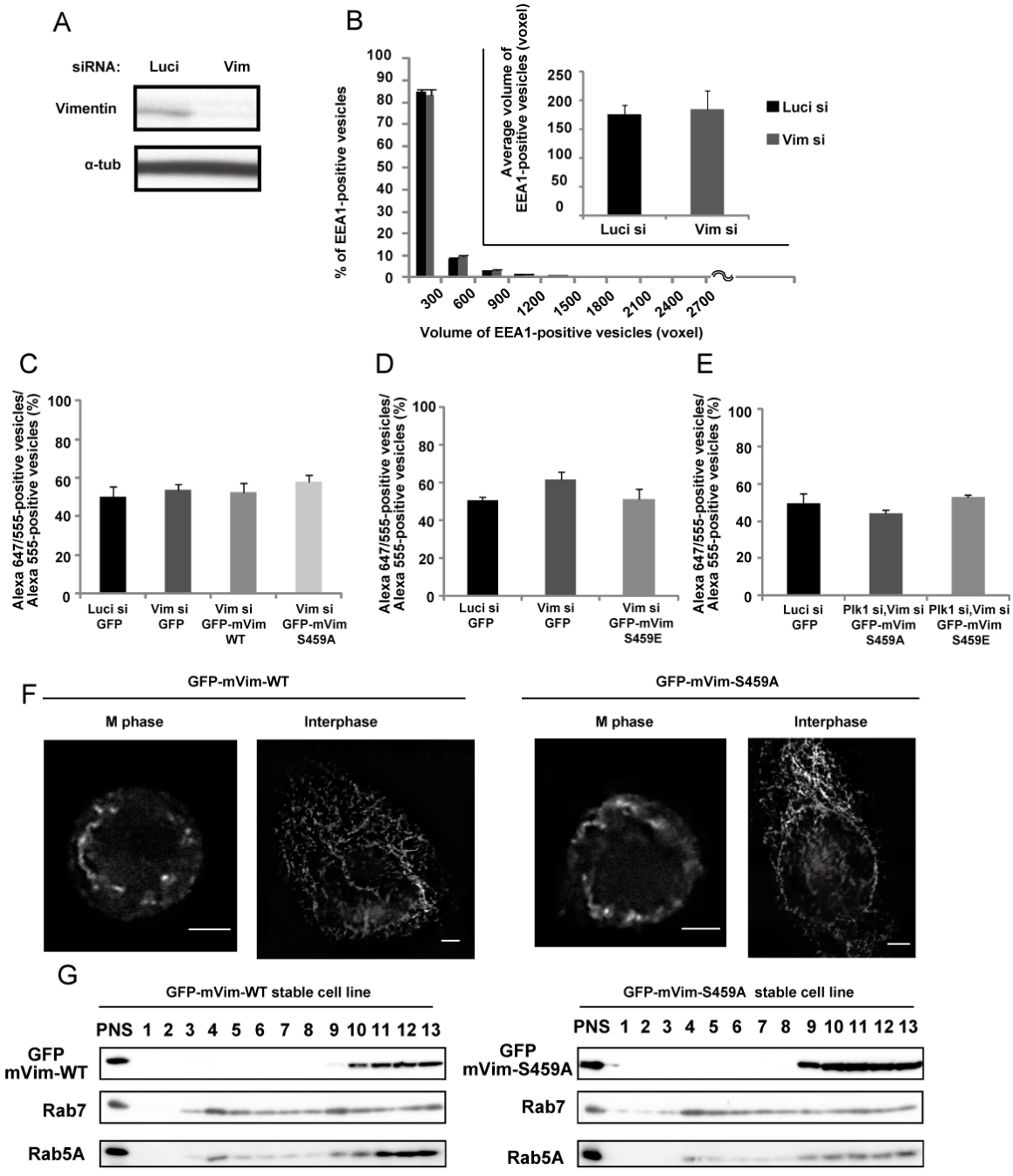

Supplementary Figure 5

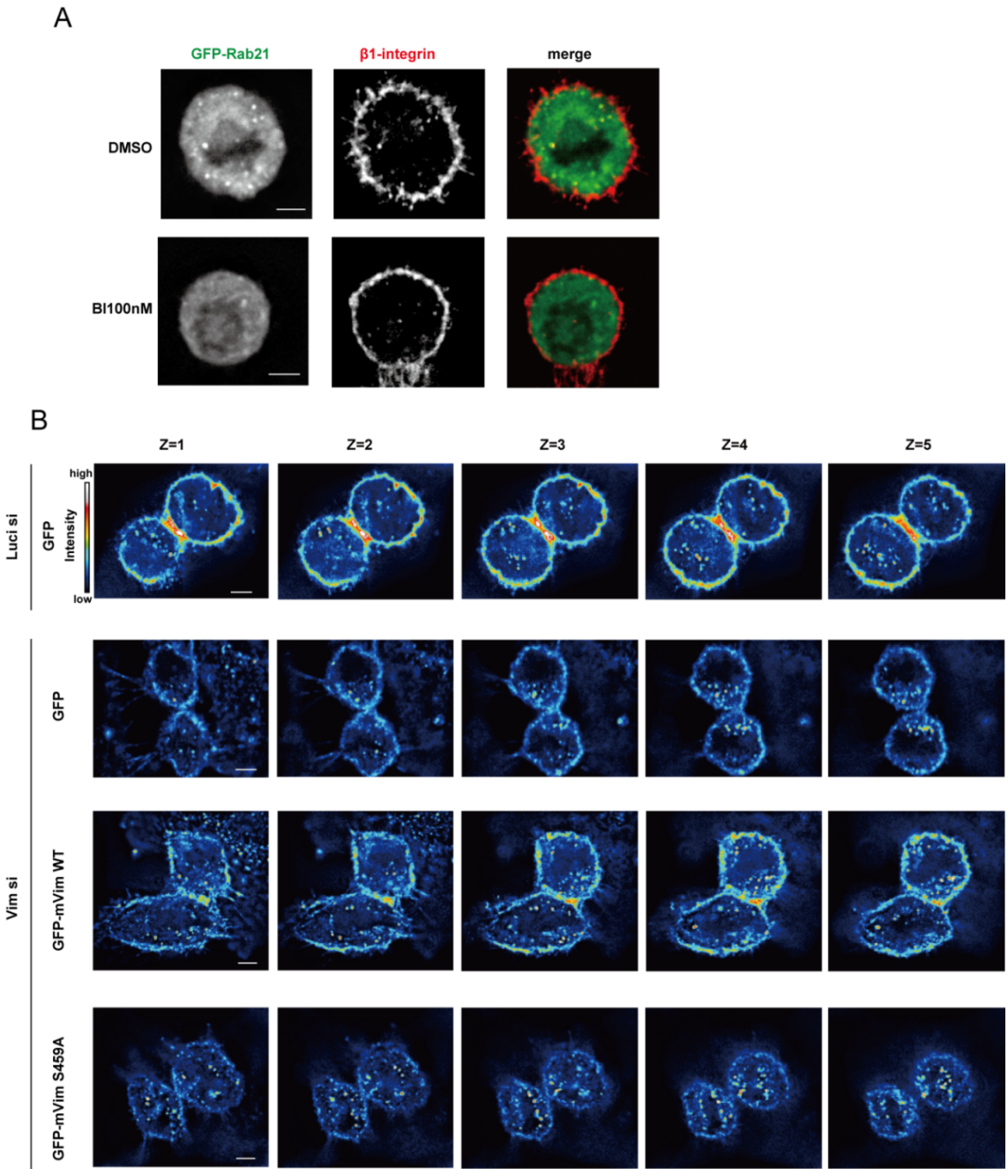

Supplementary Figure 6

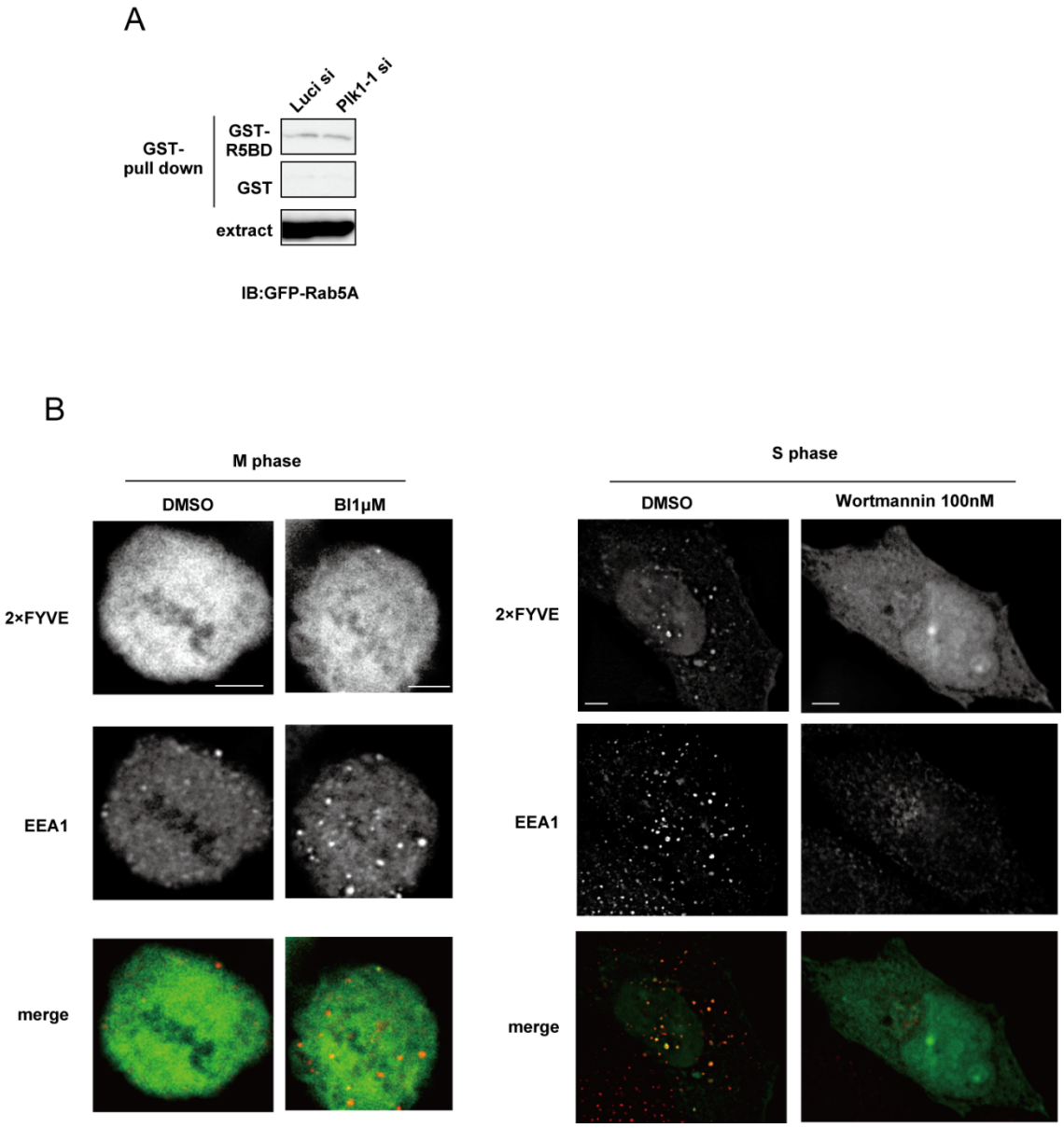

Fig. S1. Inhibition of Plk1 induces the enlargement of early endosomes during M-phase. (A) Western blot analysis for the expression of Plk1, EEA1, and control α-tubulin in M-phase synchronized cells transfected with luciferase siRNA (Luci si) or Plk1 siRNA (Plk1-1si). (B) Distribution (histogram; mean ± s.e.m. from three different experiments; n=30/experiment) and the average (inset; mean ± s.e.m. from three different experiments; n=30/experiment) volume of the EEA1-positive vesicles in the M-phase synchronized cells treated with DMSO or BI2536 (100nM) for 2 h. **P<0.01, analyzed by t-test. (C) Distribution (histogram; mean ± s.e.m. from three different experiments; n=30/experiment) and the average (inset; mean ± s.e.m. from three different experiments; n=30/experiment) volume of the EEA1-positive vesicles in the S-phase synchronized cells treated with DMSO or BI2536 (100nM) for 2 h. (D) Images of the M-phase cells transfected with the indicated siRNAs and stained with anti-CIMPR antibodies. (E) 3D construction images of CIMPR in cells in (D) (upper). Distribution (histogram; mean ± s.e.m. from three different experiments; n=30/experiment) and the average (inset; mean ± s.e.m. from three different experiments; n=30/experiment) volume of the CIMPR-positive vesicles are shown in the bottom.

Fig. S2. Depletion of NFS and α-SNAP inhibits endocytic vesicle fusion in interphase cells. (A) Images of interphase cells transfected with GFP-Rab5CA and incubated with Alexa 555-EGF for 30 min to allow endocytosis. (B) Western blot analysis of NSF, α-SNAP and control α-tubulin in cells transfected with the indicated siRNAs. (C) In-cell fusion assay in S-phase cells. S phase-arrested cells were transfected with the indicated siRNAs and incubated sequentially with Alexa 647-EGF and Alexa 555-EGF. The merged images of Alexa 647-EGF and Alexa 555-EGF in S-phase cells are shown (upper). Distribution of the volume of the Alexa 647/555-positive vesicles is shown in the histogram (n=3). A vesicle with a volume of more than 200 voxel is defined as a fused vesicle (yellow). The scale bar represents 5μm.

Fig. S3. The annotated MS/MS spectra obtained by phosphoproteome analysis in Fig. 2. (A) The annotated MS/MS spectrum of the vimentin-derived phosphopeptide in the early endosome fraction in Fig 2D. (B) The annotated MS/MS spectrum of the vimentin-derived phosphopeptide in the Plk1-vimentin reaction in Fig 2F. (C) The annotated MS/MS spectrum of the vimentin-derived phosphopeptidein the M phase-arrested cells treated with or without BI 2536 (Fig 2G) and in the cells arrested in M phase or G1/S phase (Fig 2H).

Fig. S4. Vimentin Ser459 phosphorylation is not required for vimentin filament formation or recruitment of vimentin to the early eondosome fractions. (A) Western blot analysis for vimentin and control α-tubulin in the S-phase synchronized cells transfected with the indicated siRNAs. (B) Distribution (histogram; mean ± s.e.m. from three different experiments; n=30/experiment) and the average (inset; mean ± s.e.m. from three different experiments; n=30/experiment) volume of the EEA1-positive vesicles in the S-phase synchronized cells in (A). (C) The average population of the Alexa 555-positive vesicles that are defined as docking or fused vesicles in the cells in Fig 3D (mean ± s.e.m. from three different experiments; n=30/experiment). (D) The average population of the Alexa 555-positive vesicles that are defined as docking or fused vesicles in the cells in Fig 3F (mean ± s.e.m. from three different experiments; n=30/experiment). (E) The average population of the Alexa 555-positive vesicles that are defined as docking or fused vesicles in the cells in Fig 3H (mean ± s.e.m. from three different experiments; n=30/experiment). (F) Images of GFP-WT- or S459A-mouse vimentin in M phase- (left) or S phase- (right) synchronized cells depleted with endogenous vimentin. The scale bar represents 5μm. (G) Western blot analysis for GFP-mouse WT- or S459A-vimentin, Rab7, and Rab5A in the endosome fractionations prepared from M phase arrested cells that are stably expressing GFP-mouse WT-vimentin (left) or GFP-mouse-S459A-vimentin (right). Rab7 and Rab5A are

markers for the late endosome and the early endosomes, respectively.

Fig. S5. The Plk1-vimentin pathway is required for integrin trafficking toward the cleavage furrow. (A) Cells were transfected with GFP-Rab21, synchronized in M phase and treated with DMSO or BI2536 (100 nM) for 2 h. Cells were incubated with Zenon-Alexa 546-labeled anti-β1-integrin antibodies for 30 min to allow endocytosis of the labeled antibody. The images of GFP-Rab21 and β1-integrin in metaphase cells are shown. (B) The Z-stack images (0.9μm apart) of the heat maps for the β1-integrin signals in Fig. 4D. The scale bar represents 5μm.

Fig. S6. The activation of Rab5A or endosomal accumulation of PtdIns3P are not induced in Plk1-inhibited M-phase cells. (A) GST-pull down assay for Rab5A. The M phase synchronized HeLa cells stably expressing GFP-Rab5A were transfected with the indicated siRNAs and subjected to the GST-pull down assay for Rab5A. (B) Images of M phase or S phase cells transfected with pEGFPC1-2xFYVE domain of EEA1, treated with DMSO or BI2536 (1 μM) for 2 h and stained with anti-EEA1 antibody.

Video 1. The time-lapse image of Alexa488-EGF and Alexa555-EGF in the control cell.

Video 2. The time-lapse image of Alexa488-EGF and Alexa555-EGF in the Plk1 depleted cell.